J. Fluid Mech. (1987), *vol.* 182, *pp.* 543–564
Printed in Great Britain

Natural convection in a shallow cavity

By JERRY E. DRUMMOND
Department of Mechanical Engineering, University of Akron, Akron, OH 44325, USA
AND SEPPO A. KORPELA
Department of Mechanical Engineering, The Ohio State University, Columbus, OH 43210, USA

(Received 11 September 1985 and in revised form 9 February 1987)

We present numerical solutions of natural convection in a shallow enclosure heated from a side. As a result of hydrodynamic instability transverse cells appear in the flow if the Prandtl number is sufficiently small. Both conducting and insulated top and bottom boundaries were considered. For fluids of small Prandtl number the differences in the flow patterns in these two cases are slight, the strength of the circulation in the cells being somewhat weaker when the boundaries are insulated. This is a result of a more stable flow in this case, caused by the kinetic energy being more vigorously expended in the work against the buoyant forces. Insulated boundaries allow the temperature field to adjust more freely in the end regions leading to crowding of the isotherms there and consequently to larger heat transfer than when the boundaries are conducting.

1. Introduction

In this article we discuss the natural convection in a shallow cavity with one sidewall heated and the other cooled. By shallow we mean that the aspect ratio of the cavity (defined as the height to width ratio) $A \ll 1$. The third dimension is taken to be large, so that the flow can be assumed two-dimensional. Several authors have recognized that the flow in this configuration is useful for modelling a number of physical systems. Boyack & Kearney (1972) assumed the shallow enclosure to be a good approximation of the region enclosing auxiliary cooling systems for high-temperature gas-cooled reactors and obtained numerical solutions for the flow. Hart (1972) studied the stability of this flow, and related it to Hadley circulations in planetary atmospheres. Cormack, Leal & Imberger (1974*a*) considered this geometry to be applicable in the study of dispersion of pollutants in estuaries. Hurle (1966), Hurle, Jakeman & Johnson (1974), and Gill (1974) were motivated to find out why temperature oscillations appear in this flow and whether these oscillations are the cause of undesirable properties in melt-grown crystals. Bejan & Rossie (1981) used a similar configuration to model a solar-energy storage system and to analyse the flow and its relationship to effective energy utilization in buildings.

The basic flow in a shallow cavity is quite easy to visualize. The fluid rises along the hot wall, travels along the top boundary and descends as it rejects heat to the cold wall. The cold fluid then returns to its starting point, forming a recirculation zone that fills the entire cavity (see figure 1). Although this kind of pattern also appears in tall enclosures it is obvious that for shallow cavities smaller areas exist for heating and cooling the fluid and that the top and bottom boundaries greatly influence the flow. The boundary conditions appropriate for the top and bottom

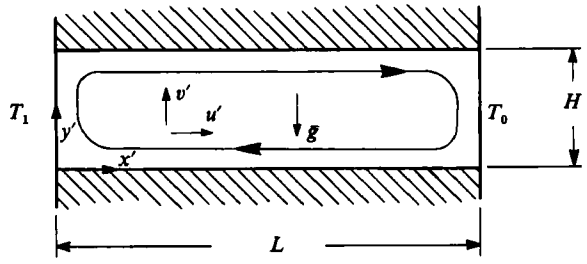

FIGURE 1. A sketch of a shallow cavity.

surfaces, such as insulating, highly conducting or free surface conditions, depend on the application.

The papers by Cormack, Leal & Seinfeld (1974*b*) and Imberger (1974), along with Cormack *et al.* (1974*a*), are important for understanding the flow in a shallow cavity. They give a theoretical analysis of the limit as the aspect ratio approaches zero. Their cavity included insulated horizontal boundaries, and in a later paper by Cormack *et al.* (1975) the work was extended to include several different conditions at the top. Using experimental and numerical techniques to verify the analytical results, they studied flows with Rayleigh numbers ranging from 7 to 2.15×10^6. The Rayleigh number is defined in this paper as $Ra = g\gamma\Delta T H^4/\nu\alpha L$, where g is the gravitational acceleration, H is the height of the cavity, and L its width; γ is the coefficient of volumetric expansion, ν the kinematic viscosity, and α the thermal diffusivity; ΔT is the temperature difference between the endwalls. For values of Rayleigh number in the lower end of the above range, they found that heat is transferred mainly by conduction so that temperature drops rather uniformly through the core of the cavity. In the core, which is the region away from the endwalls, the fluid flows parallel to the top and bottom boundaries with the result that the velocity profile there varies as a cubic polynomial in the vertical coordinate. As the Rayleigh number approaches 10^6, the size of the core region decreases markedly as does the horizontal temperature gradient in the central part of the cavity.

Bejan & Tien (1978) sought to describe the changes that occur as Ra is increased by classifying the flow into conduction, intermediate and boundary-layer regimes. These categories are based on the mechanism by which heat is transferred between the sidewalls, and are borrowed from the study of Eckert & Carlson (1961) for tall cavities. As the Rayleigh number increases, conduction, which dominates at low Rayleigh numbers, gradually diminishes and convection in the boundary layers at the vertical walls begins to control heat transfer. The intermediate regime is marked by increasing vertical stratification of the temperature in the core as Ra increases. This is noted by Imberger (1974) for $A = 0.01$ and Ra between 10^4 and 10^6. To calculate the flow in the intermediate and boundary-layer regimes, Bejan & Tien used the cubic velocity and quintic temperature profiles proposed by Cormack *et al.* (1974*a*) for the core regions and patched these to assumed solutions in the end regions.

Other authors have also addressed some aspects of this problem. Said & Trupp (1979) have contributed some numerically computed Nusselt-number data for the low-Rayleigh-number range with A as low as 0.5. Numerical solutions have also been presented by Inaba *et al.* (1981) for enclosures with aspect ratios as low as 0.03 and for moderate Rayleigh numbers ($3 < Ra < 10^6$). Shiralkar & Tien (1981) carried out a numerical study in a similar Ra-range but for fluids with Prandtl number as low

as 0.01. Sernas & Lee (1981), in addition to calculating the flow numerically, measured the heat transfer rates using interferometric techniques. The smallest aspect ratio in their experimental work was 0.1 and Ra was around 10^5. Wirtz & Tseng (1979, 1980) have concentrated on tilted cavities where $A \geqslant 0.2$.

The more recent investigations such as those of Bejan, Al-Homoud & Imberger (1981), Ostrach, Loka & Kumar (1980), Simpkins & Dudderar (1981), Shiralkar, Gadgil & Tien (1981) and Wirtz, Righi & Zirilli (1982) have dealt with large-Rayleigh-number flows ($Ra \rightarrow 10^8$). In general, they have shown that for large Ra the flow in the central part of the cavity has a very low velocity except along the top and bottom boundaries where there are wall jets. Velocity profiles look similar to those measured by Elder (1965) for the boundary-layer regime in the vertical slot. Bejan *et al.* have determined that these horizontal velocity peaks begin to appear when $Ra^{\frac{1}{4}} A^{\frac{3}{4}} > 1$.

Owing to the similarity between the flow in shallow and tall cavities, we discuss here also some of the studies of the latter. In the conduction-dominated regime the velocity is again cubic. Instability of this flow was first studied by Gershuni (1953) and later more accurate results were given by Rudakov (1967), Birikh *et al.* (1972), Korpela, Gozum & Baxi (1973) and Ruth (1979). Vest & Arpaci (1969), and Schinkel (1980) have presented experimental evidence of secondary cellular flows arising from the instability of the conduction regime, while such evidence has been presented for the boundary-layer regime by Elder (1965), Linthorst, Schinkel & Hoogendorn (1981), and Seki, Fukusako & Inaba (1978). Grondin & Roux (1979), Lauriat (1980) and Lee & Korpela (1983) have obtained the multicellular structure using numerical methods. Drifting cellular flows in a vertical annular region have been observed in experiments by Choi & Korpela (1980) and in calculations by Lee, Korpela & Horne (1982). Hart (1971) has shown that for the conduction regime at low Prandtl numbers the disturbances causing the secondary cellular flows in the vertical slot draw their energy from the base flow. The instability is hydrodynamic in origin, caused by the shear between the upward- and downward-flowing fluid streams. As the Prandtl number is increased, more of the energy comes from the buoyancy field and for $Pr > 12.7$ Korpela *et al.* (1973) found that the mode of instability changes from one of multicellular flow to a travelling-wave type. Bergholz (1978) and Lauriat & Desrayaud (1985) have discussed the stability, energy transfer mechanism and the formation of multicellular flow for the transition and boundary-layer regimes in a vertical cavity.

The linear stability theory of the parallel flow in a shallow cavity was first considered by Hart (1972) for conducting boundaries and later (Hart 1983*a*) for both rigid insulated boundaries and when the top boundary is free. He found that the instabilities can set in as transverse modes (cell axes perpendicular to the base-flow direction) or longitudinal modes (axes parallel to the base flow). In the earlier paper he noted that for low Prandtl numbers the longitudinal modes are oscillatory, which prompted Gill (1974) to investigate whether these modes are the source of temperature fluctuations in metal and semiconductor melts. Recently, part of Hart's results were recalculated by Roux, Bontoux & Henry (1984) and more extensive calculations are given by Kuo (1986) and Kuo *et al.* (1986). Kuo's results agree with the calculations of Roux *et al.* (1984), but not with the early work of Hart. Although the physical mechanisms proposed by Hart remain good, there are significant differences between his results and the later calculations.

Kuo reports that for a flow in a cavity with conducting horizontal walls, stationary transverse modes are the most unstable for $Pr < 0.14$. Longitudinal oscillating modes

take over in the range $0.14 < Pr < 0.4$, and beyond this the critical modes are longitudinal stationary ones. For insulated top and bottom the situation is similar, with the stationary transverse modes being the most unstable for $Pr < 0.033$, longitudinal oscillatory ones in the range $0.033 < Pr < 0.2$, and longitudinal stationary ones in the range $0.2 < Pr < 2$. The difference brought about by the thermal boundary condition is that, whereas in the first case the longitudinal stationary modes are destabilized as the Prandtl number is increased, in the cavity with insulated top and bottom these modes become more stable. Beyond $Pr = 2$ the flow in the cavity with insulated horizontal walls is very stable and the instability, when it occurs, is a travelling-wave type.

In this paper we present results of numerical calculations of laminar flow in shallow cavities for the following range of parameters: $\frac{1}{20} \leqslant A \leqslant \frac{1}{8}$, $Gr \leqslant 30000$, and $Pr \leqslant 2.0$. Here the Grashof number is defined as $Gr = g\gamma\Delta T H^4/L\nu^2$. These ranges permit analysis of the flow preceding and resulting from the onset of the transverse instabilities. The Gr-range has been selected such that, in general, the values governing the onset of longitudinal disturbances will be avoided. Since only transverse modes are considered, a two-dimensional rectangular cavity is employed, the horizontal boundaries being either insulated or conducting.

2. Formulation and solution

The configuration to be studied is seen in figure 1. The symbols u' and v' respectively represent the dimensional velocities in the direction of x' and y'. The vertical walls are isothermal, the hot wall at the left, and the horizontal boundaries are either insulated or conducting. The governing equations are put into dimensionless form using the scale H for length, $\Delta T = T_1' - T_0'$ for the temperature, $U = g\gamma\Delta T H^2/\nu$ for velocity, H^2/ν for time, U/H for vorticity, and UH for the stream function. All temperatures are measured above that of the cold wall. Density changes in the fluid are considered to be important only as they affect the buoyancy, and all other physical properties of the fluid are taken to be constant. Viscous dissipation is also ignored. The equations of motion and energy, written in terms of the vorticity ω, stream function Ψ, and temperature T, now become

$$\frac{\partial\omega}{\partial t} + \frac{Gr}{A} J(\omega, \psi) = \frac{\partial^2\omega}{\partial x^2} + \frac{\partial^2\omega}{\partial y^2} + \frac{\partial T}{\partial x}, \tag{1}$$

$$\frac{\partial T}{\partial t} + \frac{Gr}{A} J(T, \psi) = \frac{1}{Pr}\left(\frac{\partial^2 T}{\partial x^2} + \frac{\partial^2 T}{\partial y^2}\right). \tag{2}$$

The Poisson equation,

$$\frac{\partial^2\psi}{\partial x^2} + \frac{\partial^2\psi}{\partial y^2} = -\omega, \tag{3}$$

connects the stream function to vorticity. The vorticity and stream function are defined by the relations

$$\omega = \frac{\partial v}{\partial x} - \frac{\partial u}{\partial y}, \quad u = \frac{\partial\psi}{\partial y}, \quad v = -\frac{\partial\psi}{\partial x},$$

and the two Jacobians are given by

$$J(\omega, \psi) = \frac{\partial\omega}{\partial x}\frac{\partial\psi}{\partial y} - \frac{\partial\omega}{\partial y}\frac{\partial\psi}{\partial x}, \quad J(T, \psi) = \frac{\partial T}{\partial x}\frac{\partial\psi}{\partial y} - \frac{\partial T}{\partial y}\frac{\partial\psi}{\partial x}.$$

The above equations are subject to the following boundary conditions:

$$\psi = \frac{\partial \psi}{\partial x} = 0 \quad \text{at } x = 0, A^{-1}, \quad \psi = \frac{\partial \psi}{\partial y} = 0 \quad \text{at } y = 0, 1,$$

$$T = 1 \quad \text{at } x = 0, \quad T = 0 \quad \text{at } x = A^{-1},$$

$$\frac{\partial T}{\partial y} = 0 \quad \text{at } y = 0, 1, \quad \text{for insulated walls},$$

$$T = 1 - Ax \quad \text{at } y = 0, 1, \quad \text{for conducting walls},$$

where $A = H/L$. For the limiting case of a highly conducting fluid ($Pr = 0$), (2) is dominated by the diffusion term and the temperature profile becomes a simple linear function of x. Equations (1) and (3) then describe the fluid motion with $\partial T/\partial x = -A$, and the rest of the thermal conditions can be dropped.

Equations (1)–(3), along with the boundary conditions, were solved numerically using finite-difference techniques. The leap-frog method of DuFort & Frankel, as outlined in Roache (1972), was applied to the diffusion and time-derivative terms. This approach removes the diffusion restriction on the time-step. Jones (1979) has mentioned that the DuFort–Frankel method may result in inaccuracies for low-Prandtl-number fluids, but extensive testing of the technique by Drummond (1981) has shown that this need not be a concern in our implementation. A transient solution method is necessary owing to the possible presence of travelling-wave disturbances in the flow.

The method of Arakawa (1966) was used to approximate the Jacobians in (1) and (2) by finite differences. This method incorporates important conservation properties and is recommended by Roache (1972) for problems that involve hydrodynamic instabilities. It has been used by Festa (1970), Quon (1972), Wirtz & Liu (1975), and Cormack *et al.* (1974*b*) and it can be easily applied to explicit finite-difference equations. A two-point central difference was used for the buoyancy term.

The Poisson equation for ψ was solved by using the direct method of Buzbee, Golub & Nielson (1970), which is an offshoot of the cyclic reduction algorithm of Buneman (1969). Boundary vorticity was updated with an equation exhibiting first-order accuracy, and the temperature of the insulated wall was computed using a second-order conduction equation. Overall, equations for the interior nodes of the finite-difference mesh are second-order accurate.

The computational procedure for a single time-step was typical of that for explicit formulations with the temperature field, including boundary nodes, calculated first. This was followed by updating the vorticity and stream-function fields and finally the boundary values of vorticity. Computations were terminated by comparing vorticity fields from successive time-steps. Numerical stability was achieved by using the time-step limitation

$$\Delta t \leqslant 0.95\left[0.75\frac{Gr}{A}\left(\frac{|u_{i,j}|}{\Delta x}+\frac{|v_{i,j}|}{\Delta y}\right)\right]^{-1}, \tag{4}$$

which is a modified form of the Courant condition. Here Δx and Δy are the uniform grid spacings and $u_{i,j}$ and $v_{i,j}$ the nodal velocities. Since a leap-frog time differencing was used in the main part of the calculation, a one-step explicit routine in which the time-step is limited by

$$\Delta t \leqslant 0.95\left[\frac{2}{Pr}\left(\frac{1}{\Delta x^2}+\frac{1}{\Delta y^2}\right)+0.75\frac{Gr}{A}\left(\frac{|u_{i,j}|}{\Delta x}+\frac{|v_{i,j}|}{\Delta y}\right)\right]^{-1} \tag{5}$$

was needed to start the calculations. For low values of Prandtl number this Δt can be very restrictive even when limited to the initialization routine. To speed up the starting process in this case, the temperature field alone was updated according to the Δt of (5). The ω- and ψ-fields were not changed until the limiting time-step for the vorticity equation was reached, this being a factor of about Pr^{-1} larger than that of (5). When the limiting case of $Pr = 0$ was considered, the temperature-field calculation was by-passed and the Prandtl-number restriction on Δt did not appear.

The computations were started either from quiescent conditions or from established flow fields that had been calculated with slightly different parameters. Runs with small Prandtl numbers were normally begun with the fluid having a constant horizontal temperature gradient.

There are states for which initial conditions can influence the outcome of the flow pattern. These are for those aspect ratios for which a flow with n cells is about as likely to occur as one with $n+1$ cells. For the calculations to be discussed, the initial conditions do not influence the steady-state results. That is, the aspect ratios were such that a unique flow pattern, independent of the initial conditions, emerged.

Nusselt numbers were calculated with a conduction equation used by Lee (1981) which exhibits formal third-order accuracy. The calculations were carried out on an Amdahl 470 V/6 computer using the IBM H-Extended compiler. Normal runs used a mesh with 21 grid points in the y-direction and 65 in the x-direction and required between one and two minutes of CPU time. This translates to a requirement of 0.13–0.21 CPU-seconds for each time-step in the explicit marching sequence. Nusselt-number data presented in this paper are generally accurate to within 4%, except for certain cases in which the Prandtl number approaches 1.0. These results should be accurate to within 10%. Temperature, velocity and vorticity values are in all cases accurate to within 4%. Extensive tests for convergence and accuracy were conducted using up to 257 grid points in the x-direction, and several comparisons were made with the findings of other authors in order to verify our numerical method. Details of these tests are presented in Drummond (1981).

3. Results and discussion

In this section the results of the numerical experiments conducted for the shallow cavity are described. The effect on the flow and thermal structure of varying the Grashof and Prandtl numbers is shown by contour plots of streamlines and isotherms. In each of the plots the hot wall of the enclosure is on the left. The influence of the aspect ratio is shown undistorted by changes in the horizontal scale even in the most shallow cavities. The influence of Grashof number is presented first; this is followed by a discussion of the Prandtl-number effects. A short section is included on the heat-transfer results. Details regarding the onset of secondary flow as well as comments on the aspect-ratio effects are given in the appropriate paragraphs in the following subsections.

3.1. *Influence of Grashof number*

In figures 2 and 3 are shown contour plots of streamlines and isotherms for enclosures with conducting and insulated horizontal boundaries, respectively. In both figures, the aspect ratio is $\frac{1}{10}$ and $Pr = 0.05$ and each series of plots is shown for varying values of Gr. The flow in each cell rotates clockwise.

For fluids of small Prandtl number linear stability analysis (Hart 1972; Kuo *et al.* 1986; Kuo & Korpela 1987) shows that in an infinitely shallow cavity the

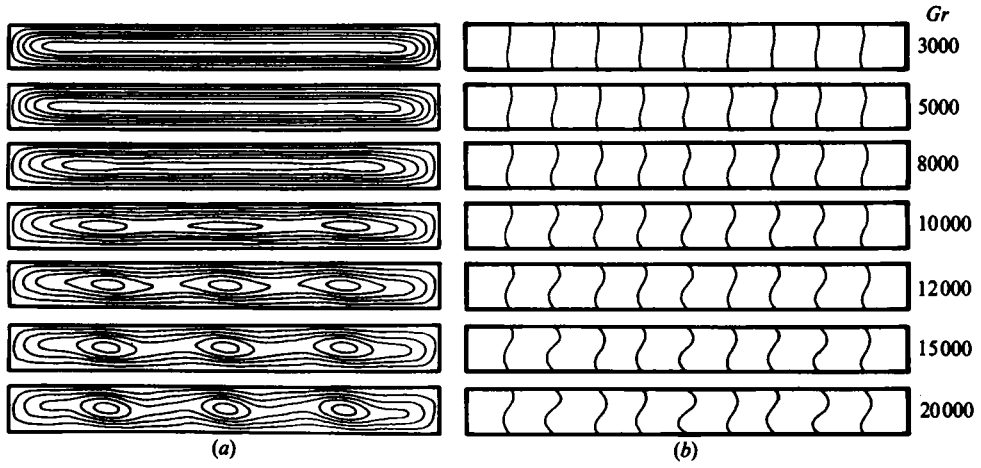

FIGURE 2. Effect of Grashof number on convection with $A = \frac{1}{10}$, $Pr = 0.05$ and conducting boundaries: (*a*) streamlines; (*b*) isotherms.

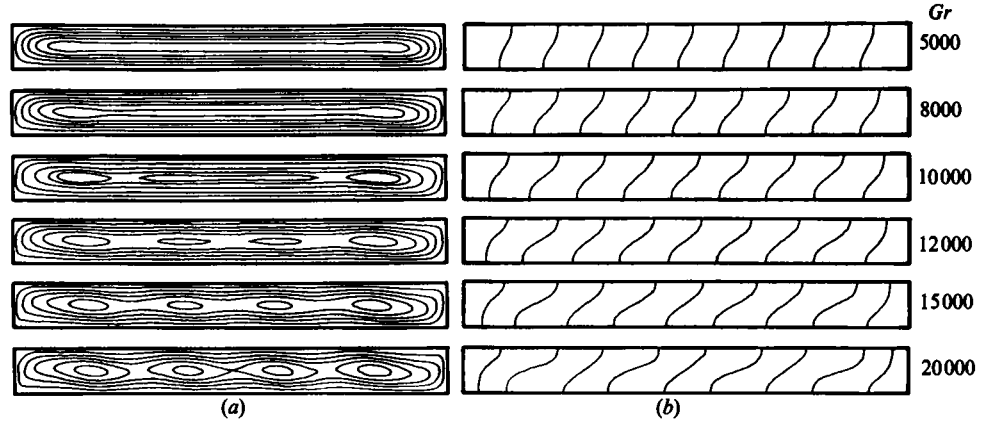

FIGURE 3. Effect of Grashof number on convection with $A = \frac{1}{10}$, $Pr = 0.05$ and insulated boundaries: (*a*) streamlines; (*b*) isotherms.

instability that arises as Gr is increased is hydrodynamic in origin, the thermal field influencing matters only slightly. Thus the onset of instability is not expected to depend greatly on which of the two thermal conditions is imposed at the horizontal boundaries. Figures 2 and 3 confirm this qualitatively. To be sure, the different temperature fields and the finite aspect ratio must influence the core flow somewhat. The strength of the cellular flow is seen to be weaker at a given Gr when the horizontal walls are insulated. For a cavity with conducting walls, an examination of the vertical velocity along the horizontal mid-plane shows that four cells are present at the onset of instability, although these are not visible in the contour plots on figure 2. At $Gr = 10000$ the two centre cells have merged and a three-cell pattern is evident. Further increase of Gr results in strengthening of the circulation in each cell. For the insulated boundaries, figure 3 shows a four-cell pattern remaining intact over the range of Gr considered. At $Gr = 20000$ the vorticity at the centre of the inner cells in the insulated enclosure is 17 % lower than that for the centre cell in the enclosure with conducting walls. That the angle of inclination of the cells with the horizontal

in the insulated cavity is smaller is further evidence of weaker secondary circulation. The reason for this weaker circulation is the greater stability of the flow with insulated boundaries. The stability calculations of Kuo *et al.* (1986, 1987) show the onset of instability for a flow in a cavity with conducting boundaries to appear at a lower value of the Grashof number than when the boundaries are insulated. We assume that qualitatively this also holds true when the aspect ratio is finite. It is tempting to appeal to a kinetic-energy balance for an explanation of why in one case the circulation is stronger. In doing so one implicitly assumes that for those cases for which the rate of production of kinetic energy is larger, the kinetic energy of the secondary flow field at steady state is also larger. This need not necessarily be true, although it is likely to be so. For the low Prandtl numbers our calculations show that all the kinetic energy of the secondary field is produced by the Reynolds stresses interacting with the mean flow; in fact, the influence of the secondary temperature field is to draw kinetic energy away from the disturbance velocity field. One can make an even stronger statement by noting that the product $vT \leqslant 0$ (where both v and T here denote variables characterizing the secondary flow) holds locally almost everywhere, so the fluid particles, as they flow, continuously do work against the buoyancy field. This effect is much more pronounced in the insulated enclosure than in the one with conducting top and bottom boundaries and leads to the weaker circulation in that case.

The balance equation for the temperature variance from the mean gives information on the causes of the distortion of the temperature field. Our calculations show that the main agent to provide the secondary thermal field with its form at steady state is the term $uT\partial\overline{T}/\partial x$, in which the overbar denotes the base temperature. Indeed, its vertically integrated value, for a fluid of $Pr = 0.05$, is an order of magnitude greater than the integrated $vT\partial\overline{T}/\partial y$ term associated with the vertical motions.

In figure 4 the vorticity in the end and centre cells is plotted as a function of Grashof number for a fluid of $Pr = 0$. The aspect ratio $A = \frac{1}{8}$ is such that a stable three-cell pattern is present for all values of Gr. The outer cells are seen to develop gradually as Gr increases, having started in the turning regions at the ends of the cavity. The centre cell develops more suddenly at $Gr \approx 7000$. This is an indication of an imperfect bifurcation of the solution.

A detailed analysis by Daniels, Blythe & Simpkins (1986) shows that for fluids of $Pr < 0.12$ the convective flow in a cavity with insulated top and bottom undergoes an imperfect bifurcation, but if $Pr > 0.12$ this does not happen. Our calculations are consistent with their conclusions and further evidence is shown in figure 5. Although the figure is for a flow in a cavity with conducting boundaries, similar behaviour is expected for small Prandtl numbers when the boundaries are insulated. In the figure are shown vertical velocities along the horizontal centreline for a flow at $Gr = 8000$ in a cavity with $A = \frac{1}{15}$. The strength of the circulatory flow in the end cell is seen to diminish as the Prandtl number is increased from zero to 0.1, and at $Pr = 0.2$ the secondary flow has vanished.

The possibility of an imperfect bifurcation was put forth by Hart (1983*b*) in a numerical study. He saw, as we do, the cells to gain in strength as the end is approached. However, he forced the flow to be parallel away from the ends. This condition cannot be imposed on the cellular flow because the cells, when allowed to develop freely, become skewed with odd symmetry about the centre point of the isotherms of figures 2 and 3. In both cases the cold fluid moving to the left in the

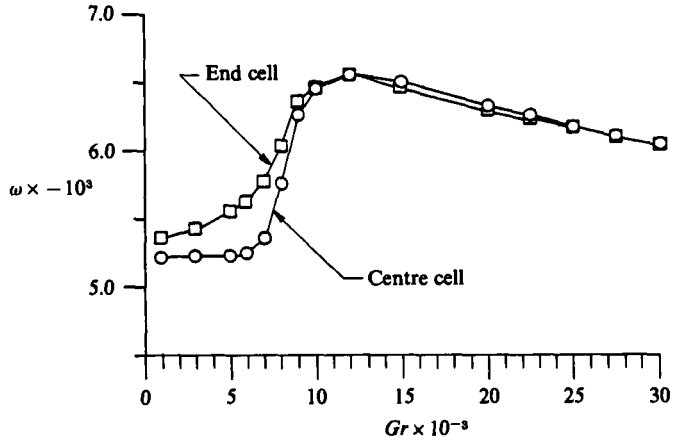

FIGURE 4. Vorticity at the centre of cellular regions for $A = \frac{1}{8}$, $Pr = 0$.

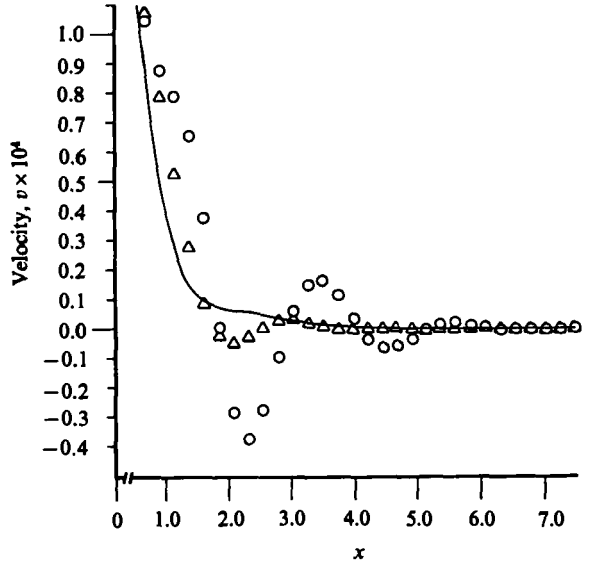

FIGURE 5. Variation of the vertial velocity at the horizontal centreline of the cavity with the distance from the hot end for $Gr = 8000$ and $A = \frac{1}{15}$: ○, $Pr = 0$; △, 0.1; ——. 0.2.

for the flow to undergo a transition to a multicellular pattern in the core region, and thus accentuates the successive build-up of eddies from the ends to the centre.

In figure 6 we show further behaviour of the flow of a zero-Prandtl-number fluid for increasing Gr. The centre cells are seen to be very weak at $Gr = 7000$–8000 (near the onset of instability) and the two centre cells move closer together and eventually merge near $Gr = 10000$. As Gr increases beyond 10000 the cells become stronger and begin to tilt. Small circulation patterns, visible at $Gr = 12000$, form between the large established cells. Figure 7 shows a detail of the region between the cells and the circulation is noted to be in the same direction as in the large cells. The small eddy appears to be the result of shear from opposing streams and could be considered to be a secondary instability. These small cells then grow and eventually take their place

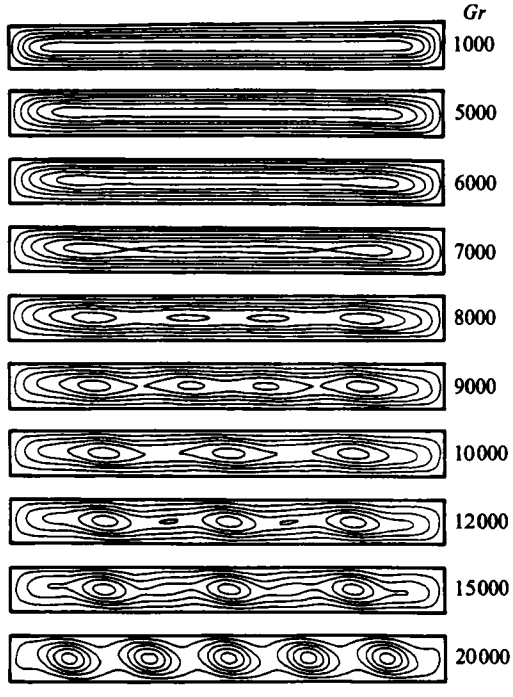

FIGURE 6. Effect of Grashof number on streamline pattern for $A = \frac{1}{10}$ and $Pr = 0$.

FIGURE 7. Detail of intercellular rotation.

in the secondary-flow pattern as full-sized cells when $Gr = 20000$. One can question whether this kind of instability actually occurs in a laboratory. It could well be that it is an artifice of the two-dimensional simulation. Secondary instabilities could lead to three-dimensional motions which our two-dimensional study cannot address.

The spacing of the cells depends on a number of factors. First is the natural spacing predicted by the stability theory for an infinitely shallow cavity. Secondly, an integral number of cells must fit into a cavity of finite aspect ratio, and the cell spacing must accommodate this constraint. The third factor is the magnitude of the departure from the onset of instability. Fourth is the extent of the end regions and how this changes with both Grashof and Prandtl numbers. In figure 8 the net result of these effects is shown. Three cells fit well into a cavity with $A = \frac{1}{8}$. By changing the aspect ratio to $A = \frac{1}{11}$ there is ample room for the fourth cell and the cell spacing is on the average larger. The initial decrease in the cell spacing as Grashof number is increased is apparently related to the flow in the end regions. As Gr is increased well beyond the onset of instability the cell spacing keeps increasing. If this increase in spacing is large enough to allow new cells to fit into the pattern, then shear between the cells will cause those new cells to form as is shown in figure 6. For some aspect ratios small intercellular rotations formed but did not grow owing to lack of space.

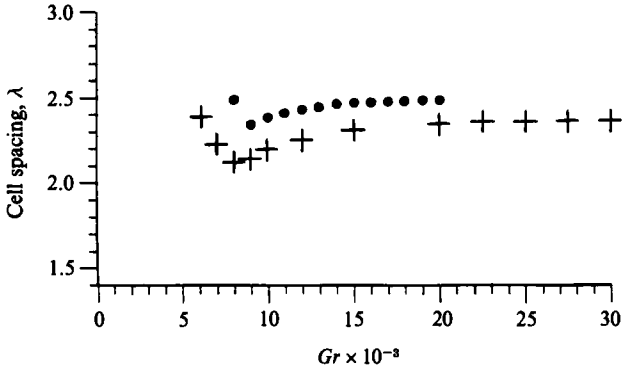

FIGURE 8. Effect of Grashof number on wavelength for $Pr = 0$: ●, $A = \frac{1}{11}$; +, $\frac{1}{8}$.

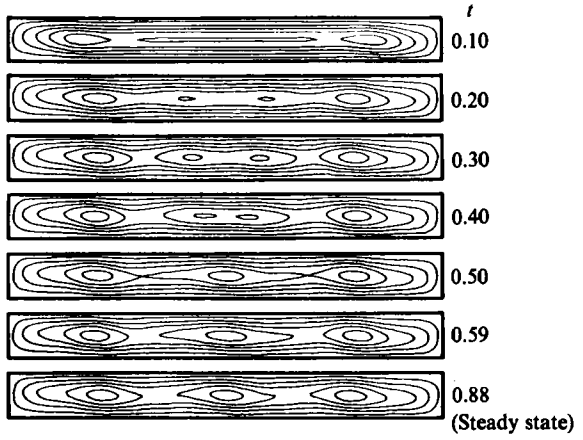

FIGURE 9. A transient development of the flow patterns with $A = \frac{1}{10}$, $Gr = 10000$ and $Pr = 0$.

An example of the temporal development of the cells is shown in figure 9. Note that the eddies at the ends of the cavity form first, symmetrically in response to the linear horizontal temperature gradient imposed as an initial condition. The cells at the centre of the enclosure grow more slowly and move closer together as time progresses until they merge sometime between $t = 0.4$ and 0.5 (dimensionless time). When steady state is reached, the cells are of uniform size and the vorticity at their centres is nearly the same.

As a final observation on the effect of Grashof number, we show in figure 10 its influence on heat transfer. The ordinate gives the Nusselt number based on cavity length, for we have defined $Nu = hH/k$, where h is the heat-transfer coefficient and k is the thermal conductivity. As will be seen later, this form of Nusselt number allows better comparison of heat transfer in cavities of different aspect ratio. It is obvious that a larger Gr would give a larger Nu/A, but the interesting point is the effect of the boundary conditions. With insulated boundaries, the Nu/A value grows much faster than when the boundaries are conducting. The reason for this is seen from the isotherms of figures 2 and 3. In both cases the cold fluid moving to the left in the lower part of the cavity is heated by the hotter fluid, which moves to the right in the upper half. If the boundaries are conducting the cold fluid also receives thermal energy from the lower boundary. The latter mechanism is absent when the boundaries

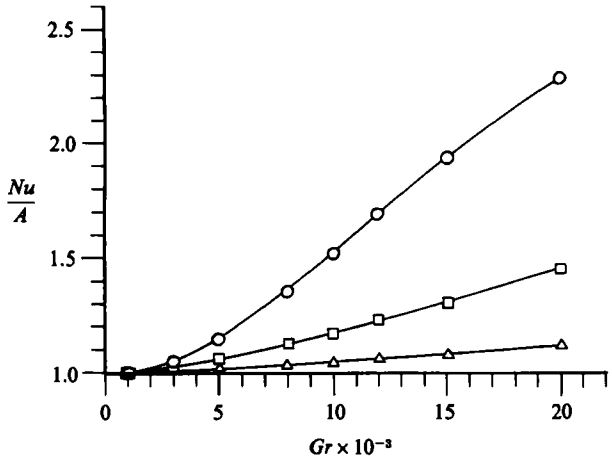

FIGURE 10. Effect of Grashof number on heat transfer with $A = \frac{1}{10}$: △, $Pr = 0.05$ with conducting walls; □, $Pr = 0.1$ with conducting walls; ○, $Pr = 0.05$ with insulated walls.

are insulated and for this case the fluid is therefore colder as it enters the end region. This leads to crowding of the isotherms in the bottom half of the hot wall and as a result to a higher heat flux there.

The local thermal field is also altered somewhat by the cells. Where the streamlines are crowded, and hence the flow is faster, the isotherms are distorted most. For a finite Prandtl number, the finite timescale for thermal diffusion allows a faster moving fluid particle to move further in a unit of time before its temperature rises by a given amount than a slower moving fluid particle can. Thus, the isotherms are further apart in the regions of crowded streamlines.

3.2. *Prandtl-number effects*

The influence of Prandtl number on the flow in a cavity with conducting boundaries is shown in figure 11. In these plots the aspect ratio is held fixed at $A = \frac{1}{8}$ and the Grashof number is likewise constant with a value $Gr = 10000$. One knows from the results of stability analysis that the flow becomes more stable to the stationary transverse modes as the Prandtl number increases. The analysis of the energetics of the flow shows that the work done by the fluid particles against the force of buoyancy increases with Prandtl number, causing the amplitude of the secondary convection to diminish and at $Pr > 0.12$ the multicellular flow to disappear completely. Kuo's (1986) analysis of the flow with insulated boundaries shows that for $0.033 < Pr < 0.20$ a longitudinal mode is the most unstable one. The competition between transverse and longitudinal modes in this range of Prandtl numbers is likely to lead to three-dimensional flows, invalidating two-dimensional calculations.

For $Pr > 0.5$ thermal boundary layers have developed along the sidewalls of the cavity and since most of the temperature drop takes place across them, the temperature gradient across the core diminishes. In figure 12 the horizontal gradient at the point in the centre is plotted as a function of Prandtl number. From that figure it is seen that for $Pr \geqslant 0.5$ the temperature gradient already behaves as it does for large Prandtl numbers and that the conduction-dominated regime extends only up to this value of Prandtl number. In figure 13 the cell spacing λ is plotted as function of Prandtl number. The value of λ decreases as Prandtl number is increased for

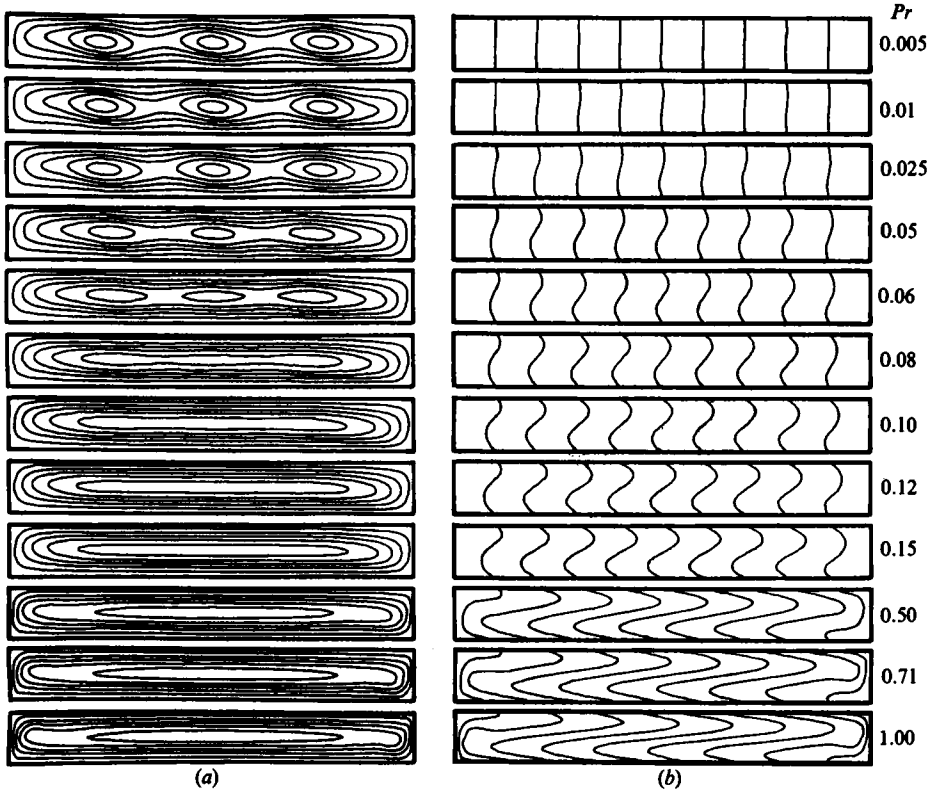

FIGURE 11. Effect of Prandtl number on convection with $A = \frac{1}{8}$, $Gr = 10000$ and conducting boundaries: (*a*) streamlines; (*b*) isotherms.

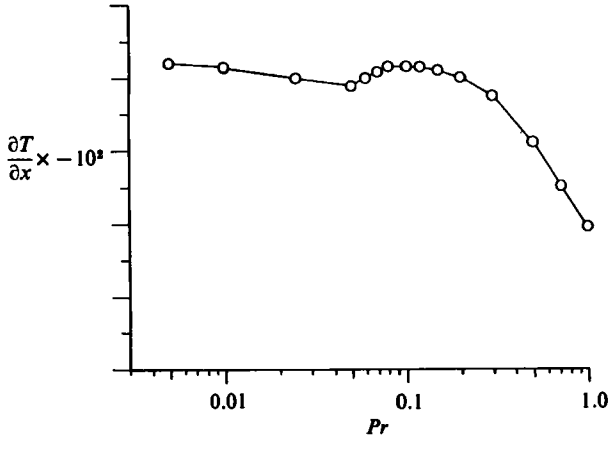

FIGURE 12. Effect of Prandtl number on the horizontal temperature gradient at the centre of the cavity for $A = \frac{1}{8}$, $Gr = 10000$ and conducting boundaries.

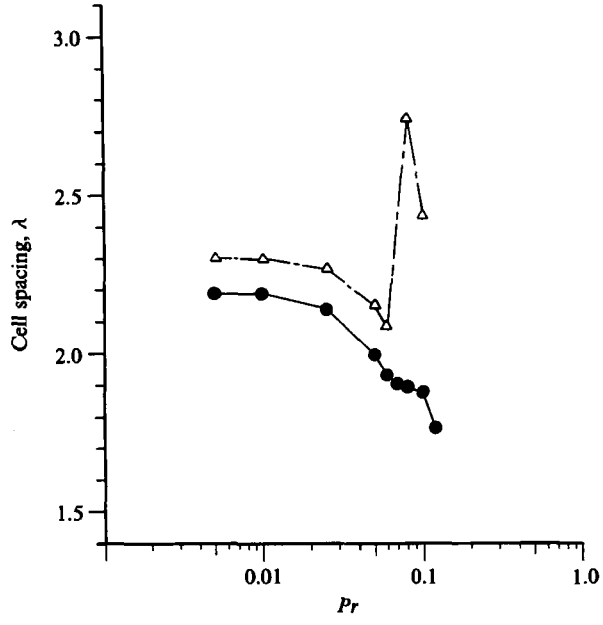

FIGURE 13. Effect of Prandtl number on the wavelength for $A = \frac{1}{8}$ and conducting boundaries: ●, $Gr = 10000$; △, 15000.

$Pr \leqslant 0.06$ for both Gr-values shown. This is observable to some extent in figure 11. For $G = 10000$, the wavelength continues to decrease with increasing Pr, but figure 14 shows that the centre cell in the original three-cell pattern disappears at $Gr = 15000$, a casuality of the end regions becoming larger at the larger values of Pr. The wavelength of the two remaining cells again begins to decrease as Pr increases. The contribution of the end regions to reducing the cell spacing is seen even more clearly from figure 15, which corresponds to the conditions $A = \frac{1}{15}$ and $Gr = 15000$. Other qualitative features are the same as before except that there are now five cells in the flow and this number remains the same for all values of Pr considered.

For flows in cavities with conducting boundaries, Hart (1972) found transverse travelling modes to be the most dangerous whenever $Pr > 0.05$. We have not been able to produce flows that correspond to his theory and recent reworking of the stability calculations for an infinitely shallow cavity by Kuo *et al.* (1986), carried to high accuracy, leads us to believe that the travelling-wave mode does not set in until $Pr > 1.5$ when $Gr = 15000$. The stability analysis is not entirely conclusive in this case because the finiteness of the aspect ratio causes the velocity and temperature profiles to deviate from the analytical ones used in the stability calculations, and this would contribute to inaccuracies in the determination of numerical values for the parameters that characterize neutral states. For conducting boundaries Hart's velocity and temperature profiles, adjusted to our scaling, are

$$u = \frac{A}{12}(-2y^3+3y^2-y), \tag{6}$$

$$T = 1-Ax+\frac{Ra\,A}{24}(\tfrac{1}{5}y^5-\tfrac{1}{2}y^4+\tfrac{1}{3}y^3-\tfrac{1}{30}y). \tag{7}$$

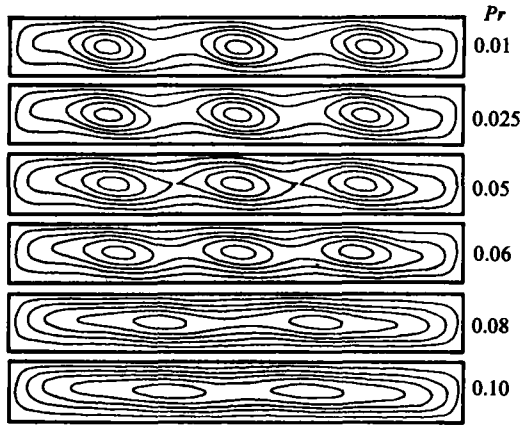

FIGURE 14. Effect of Prandtl number on stream pattern for $A = \frac{1}{8}$, $Gr = 15000$ and conducting walls.

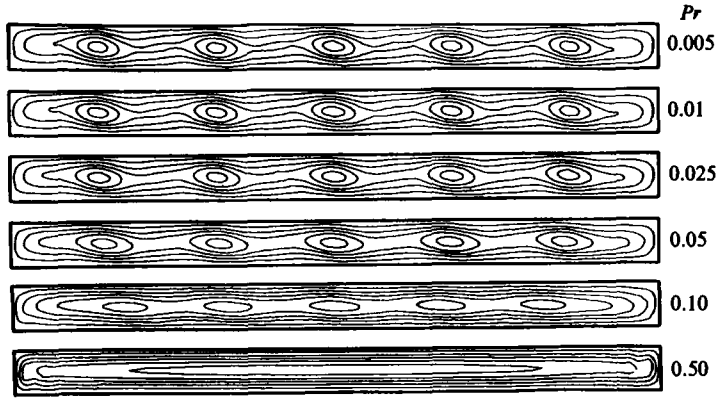

FIGURE 15. Effect of Prandtl number on stream pattern for $A = \frac{1}{15}$, $Gr = 15000$ and conducting walls.

These are compared to the numerical solutions at the vertical mid-plane of the cavity in figure 16. The results are for $A = \frac{1}{8}$, $Pr = 0.1$ and $Gr = 10000$. One can see that the agreement is excellent. This set of parameters corresponds to a flow in which stationary cells are nearly damped out owing to the large value of the Prandtl number, but the same good agreement was observed at Gr-values near the critical point. It is not surprising then that the stationary transverse cells appear at very nearly the same value of Gr in the present study as that predicted by linear stability theory. It should be mentioned that in the case of insulated boundaries the profiles used by Hart (1972, 1983*b*) deviate substantially from our numerical results for the parameters of figure 16, although they were in good agreement near the critical Gr. On the other hand the profiles proposed by Cormack *et al.* (1974*b*) and revised by Bejan & Tien (1978) were close to our numerical results in the insulated cavity for all parameter values studied.

As the Prandtl number is increased further, the base profiles begin to sharply

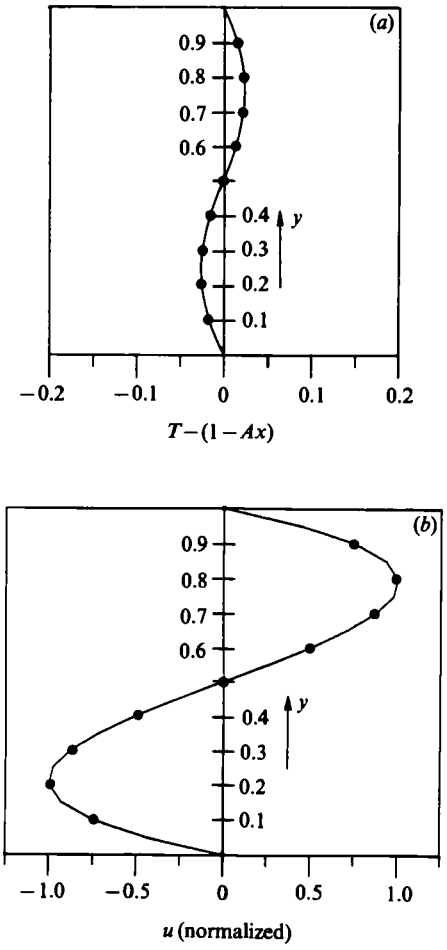

FIGURE 16. (*a*) Temperature and (*b*) velocity data at the cavity mid-point for $A = \frac{1}{8}$, $Pr = 0.1$, $Gr = 10000$ and conducting boundaries: ●, computed data; ——, profile used by Hart (1972).

deviate from the computed results as seen in figure 17 for $A = \frac{1}{10}$, $Pr = 1.0$, and $Gr = 10000$. The nature of the deviation suggests that the finite aspect ratio tends to stabilize the flow. The velocities for $A = \frac{1}{15}$ are also plotted and these are closer to the analytical expression of Hart.

By decreasing the aspect ratio further a closer match is achieved. Figure 18 shows the analytical profiles to coincide with the numerical data for air at $Gr = 6500$ and $A = \frac{1}{20}$. The curves are still reasonably close to the data when Gr is increased to 11500. Since 6500 is fairly close to the critical value of Grashof number calculated by Hart, we can conclude that stability analysis with these profiles ought to give reliable values for the critical states. This reinforces our observations that the lack of travelling waves in this cavity is not the result of the distortion of the base profiles by the end effects, and that the travelling modes are in fact damped for these values of parameters. This is consistent with the stability calculations of Kuo *et al.* (1986).

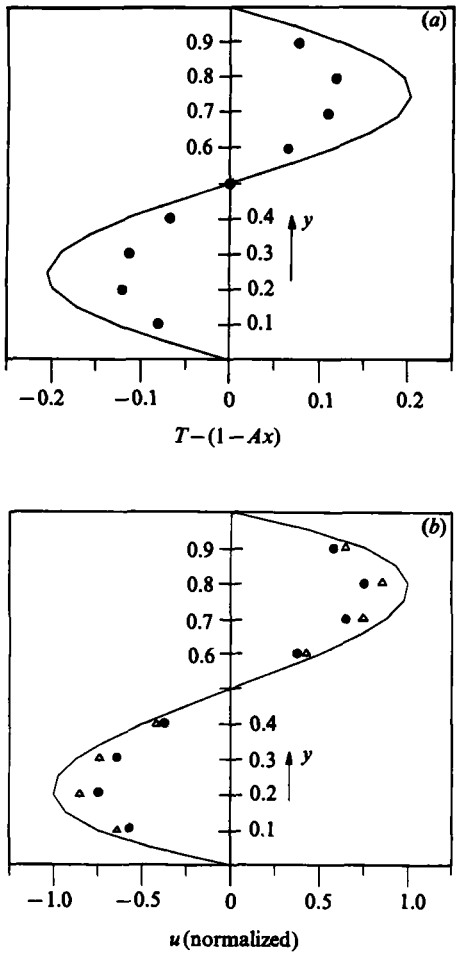

FIGURE 17. (*a*) Temperature and (*b*) velocity data at the cavity mid-point for $Pr = 1.0$, $Gr = 10000$ and conducting boundaries: ●, computed data for $A = \frac{1}{16}$; △, computed data for $A = \frac{1}{18}$; ——, profile used by Hart (1972) for all aspect ratios.

3.3. *Heat-transfer results*

In figure 19 is shown a portion of the heat-transfer data computed for the low-aspect-ratio enclosures. For purposes of comparison the Nusselt number based on cavity length, Nu/A, is plotted against Ra. The dotted and solid lines represent the correlations of Bejan & Tien (1978) for the conduction and intermediate regimes in a cavity with insulated horizontal boundaries and $A = \frac{1}{10}$. The equations for these two curves are, respectively,

$$\frac{Nu}{A} = 1 + \frac{1}{362\,880} Ra^2, \tag{8}$$

$$\frac{Nu}{A} = 1 + \left\{\left(\frac{Ra^2}{362\,880}\right)^s + \left(\frac{0.623\,Ra^{\frac{1}{5}}}{A^{\frac{4}{5}}}\right)^s\right\}^{1/s}, \tag{9}$$

where $s = -0.386$. Equation (9) is constructed in such a way that the two curves coincide at low values of Ra, as they should.

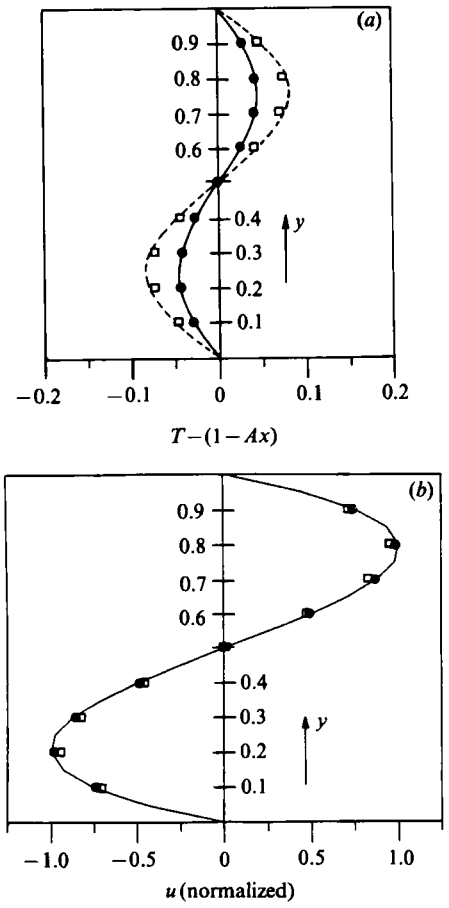

FIGURE 18. (*a*) Temperature and (*b*) velocity data at the cavity midpoint for $A = \frac{1}{20}$, $Pr = 0.71$, and conducting boundaries: ●, computed data for $Gr = 6500$; □, computed data for $Gr = 11500$; ——, profile used by Hart (1972) for velocity at all Gr and temperature at $Gr = 6500$; – – – –, Hart's temperature profile at $Gr = 11500$.

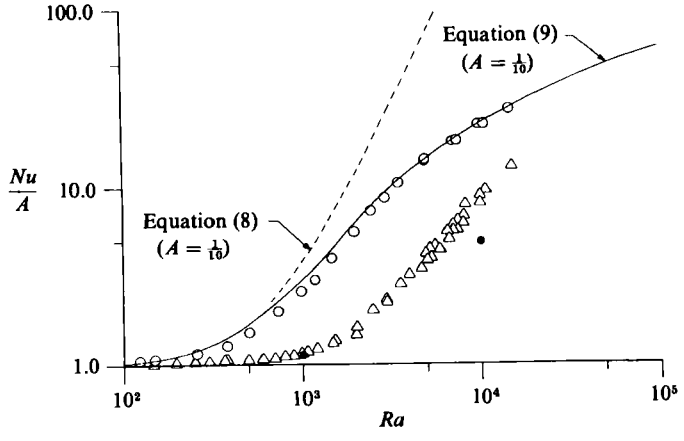

FIGURE 19. Variation of Nusselt number with Rayleigh number: ○, insulated walls, $A = \frac{1}{10}$; △, conducting walls, $A = \frac{1}{8}, \frac{1}{10}, \frac{1}{12}, \frac{1}{15}$; ●, conducting walls, $A = \frac{1}{5}$.

Our numerical results for the insulated cavity with $A = \frac{1}{10}$ are seen to fall very close to the plot of (9). Data for the conducting-wall cavity fall substantially below either curve. In this case the data include values for aspect ratios ranging from $\frac{1}{15}$ to $\frac{1}{8}$. Two points for $A = \frac{1}{5}$ show that aspect ratio affects the results somewhat, although this cannot be discerned from the bulk of the data for the conducting case. That larger aspect ratios yield lower Nu/A values was also shown by Bejan & Tien for the insulated cavity.

Since multicellular flow is absent for most of the data represented in this figure, the role of the cellular structure on the overall heat transfer is not apparent from these results. The effect of the cells would be to decrease the heat transfer because they mix momentum and temperature between the two oppositely flowing streams and thereby reduce the flow rate in each stream for a fixed driving potential. That the data are seen to fall below the curve for the lower values of Rayleigh number is consistent with this observation.

As shown in figures 10 and 19, heat transfer is increased by the presence of insulated walls which enhance thermal stratification. This causes the Nusselt number in this case to increase more rapidly with Gr than when the boundaries are conducting.

4. Conclusions

A detailed numerical study of the secondary flow in a shallow cavity has been carried out. For low-Prandtl-number fluids, secondary flow is seen to appear near $Gr = 7000$ in the form of stationary transverse cells. The critical Grashof number does not depend significantly on whether the horizontal boundaries are conducting or insulated for the reason that the instability arises from the shear and not from the buoyancy field. When $Pr > 0.01$ the cells in the insulated cavity are noticeably weaker than those for the conducting case. The difference is the result of the greater tendency for the buoyant field to draw kinetic energy from the base flow when the cavity has insulated horizontal boundaries, thus leading to a more stable flow.

The gradual onset of secondary cells for low-Prandtl-number fluids and a critical Grashof number lower than the $Gr = 8000$ predicted by linear stability theory suggest that the onset of secondary flow is the result of an imperfect bifurcation caused by the finite aspect ratio. This agrees with the analysis of Daniels *et al.* (1986), who determined that the solution bifurcates imperfectly for fluids with $Pr < 0.12$ in cavities with insulated horizontal walls. Our work shows evidence of this also for a flow in a cavity with conducting walls, and that as Prandtl number is increased beyond 0.12 the influence of the ends in causing a multicellular flow has disappeared. For these Prandtl numbers, although the cells at the ends start to form at slightly lower Gr than those closer to the centre and are stronger near the critical Grashof number, the interior cells seem to form independently and not as a sequential build-up from the ends toward the centre as Gr is increased.

Spacing of the cells in the cavity has been shown to depend on Gr, Pr and A. Cases were found for which new cells form and grow between existing cells as the space permits, the rotation dictated by the shear of the main stream. Other cases show cells merging or splitting as the spacing allows. The effect of increasing Pr is to stabilize the flow so that for $Pr > 0.12$ with $A = \frac{1}{8}$ and $\frac{1}{10}$ no secondary motions were found for the cases considered.

The heat transfer across an insulated cavity was found to be larger, at the same value of Rayleigh number, than in the cavity constructed from a material of large

conductivity. The values calculated were also shown to match the results of Bejan & Tien (1978) for the insulated cavity.

We wish to thank the Instructional and Research Computer Center of the Ohio State University for computer time and the Heat Transfer Program of the National Science Foundation for partial support of this work. While our paper was being reviewed, Professor Philip Blythe made available to us a manuscript co-authored by him. This was of benefit to us during the revision, as were the discussions with our colleague Yann Guezennec. Finally, we thank the referees for their criticism, which clarified certain points in the work.

REFERENCES

ARAKAWA, A. 1966 Computational design for long-term numerical integration of the equations of fluid motion: two dimensional incompressible flow, Part I. *J. Comp. Phys.* **1**, 119–143.

BEJAN, A., AL-HOMOUD, A. A. & IMBERGER, J. 1981 Experimental study of high-Rayleigh number convection in a horizontal cavity with different end temperatures. *J. Fluid Mech.* **109**, 283–299.

BEJAN, A. & ROSSIE, A. N. 1981 Natural convection in a horizontal duct connecting two fluid reservoirs. *Trans. ASME* C: *J. Heat Transfer* **103**, 108–113.

BEJAN, A. & TIEN, C. L. 1978 Laminar natural convection heat transfer in a horizontal cavity with different end temperatures. *Trans. ASME* C: *J. Heat Transfer* **100**, 641–647.

BERGHOLZ, R. F. 1978 Instability of steady natural convection in a vertical fluid layer. *J. Fluid Mech.* **84**, 743–768.

BIRIKH, R. V., GERSHUNI, G. Z., ZHUKHOVITSKII, E. M. & RUDAKOV, R. N. 1972 On oscillatory instability of plane parallel convective motion in a vertical channel. *Prikl. Math. Mekh.* **36**, 745–748.

BOYACK, B. E. & KEARNEY, D. W. 1972 Heat transfer by laminar natural convection in low aspect ratio cavities. *ASME Paper* 72-HT-52.

BUNEMAN, O. 1969 A compact non-iterative Poisson solver. *SUIPR Rep.* 294. Stanford University.

BUZBEE, B. L., GOLUB, G. H. & NIELSON, C. W. 1970 On direct methods for solving Poisson's equations. *SIAM J. Numer. Anal.* **7**, 627–656.

CHOI, I. G. & KORPELA, S. A. 1980 Stability of the conduction regime of natural convection in a tall vertical annulus. *J. Fluid Mech.* **99**, 725–738.

CORMACK, D. E., LEAL, L. G. & IMBERGER, J. 1974*a* Natural convection in a shallow cavity with differentially heated end walls. Part 1. Asymptotic theory. *J. Fluid Mech.* **65**, 209–229.

CORMACK, D. E., LEAL, L. G. & SEINFELD, J. H. 1974*b* Natural convection in a shallow cavity with differentially heated end walls. Part 2. Numerical solutions. *J. Fluid Mech.* **65**, 231–246.

CORMACK, D. E., STONE, G. P. & LEAL, L. G. 1975 The effect of upper surface conditions on convection in a shallow cavity with differentially heated end walls. *Intl J. Heat Mass Transfer* **18**, 635–648.

DANIELS, P. G., BLYTHE, P. A. & SIMPKINS, P. G. 1987 Onset of multicellular convection in a shallow laterally heated cavity. *Proc. R. Soc. Lond.* A **411**, 327–350.

DRUMMOND, J. E. 1981 A numerical study of natural convection in shallow cavities. Ph.D. dissertation, Department of Mechanical Engineering, The Ohio State University.

ECKERT, E. R. G. & CARLSON, W. O. 1961 Natural convection in an air layer enclosed between two vertical plates with different temperatures. *Intl J. Heat Mass Transfer* **2**, 106–120.

ELDER, J. W. 1965 Laminar free convection in a vertical slot. *J. Fluid Mech.* **23**, 77–98.

FESTA, J. F. 1970 A numerical model of a convective cell driven by non-uniform horizontal heating. Thesis, Massachusetts Institute of Technology.

GILL, A. E. 1974 A theory of thermal oscillations in liquid metals. *J. Fluid Mech.* **64**, 577–588.

GERSHUNI, G. Z. 1953 Stability of plane convective motion of a liquid. *Sov. Phys. Tech. Phys.* **23**, 1838–1844.

GRONDIN, J. C. & ROUX, B. 1979 Recherche de correlations simples experimant les pertes convectives dans une cavite bidimensionelle, inclinee, chauffee differentiellement. *Revue Phys. Appl.* **14**, 49–56.

HART, J. E. 1971 Stability of the flow in a differentially heated inclined box. *J. Fluid Mech.* **47**, 547–576.

HART, J. E. 1972 Stability of thin non-rotating Hadley circulations. *J. Atmos. Sci.* **29**, 687–697.

HART, J. E. 1983*a* A note on the stability of low-Prandtl number Hadley circulations. *J. Fluid Mech.* **132**, 271–281.

HART, J. E. 1983*b* Low Prandtl number convection between differentially heated end walls. *Intl J. Heat Mass Transfer* **26**, 1069–1074.

HURLE, D. T. J. 1966 Temperature oscillations in molten metals and their relationship to growth striae in melt-grown crystals. *Phil. Mag.* **13**, 306–310.

HURLE, D. T. J., JAKEMAN, E. & JOHNSON, C. P. 1974 Convective temperature oscillations in molten gallium. *J. Fluid Mech.* **64**, 565–576.

IMBERGER, J. 1974 Natural convection in a shallow cavity with differentially heated end walls. Part 3. Experimental results. *J. Fluid Mech.* **65**, 247–260.

INABA, H., SEKI, N., FUKUSAKO, S. & KANAYAMA, K. 1981 Natural convective heat transfer in a shallow rectangular cavity with different end temperatures. *Numer. Heat Transfer* **4**, 459–468.

JONES, I. P. 1979 A numerical study of natural convection in an air-filled cavity: comparison with experiment. *Numer. Heat Transfer* **2**, 193–213.

KORPELA, S. A., GOZUM, D. & BAXI, C. B. 1973 On the stability of the conduction regime of natural convection in a vertical slot. *Intl J. Heat Mass Transfer* **16**, 1683–1690.

KUO, H. P. 1986 Stability and finite amplitude natural convection in a shallow cavity with horizontal heating. Ph.D. dissertation, The Ohio State University.

KUO, H. P., KORPELA, S. A., CHAIT, A. & MARCUS, P. S. 1986 Stability of natural convection in a shallow cavity. In *Heat Transfer 1986, Proc. 8th Intl Heat Transfer Conf., San Francisco*, vol. 4, pp. 1539–1544. Hemisphere.

KUO, H. P. & KORPELA, S. A. 1987 Stability and finite amplitude natural convection in a shallow cavity with insulated top and bottom and heated from a side. *Phys. Fluids.* (submitted).

LAURIAT, G. 1980 Numerical study of natural convection in a narrow vertical cavity: an examination of high-order accurate schemes. *ASME Paper* 80-HT-90.

LAURIAT, G. & DESRAYAUD, G. 1985 Natural convection in air-filled cavities of high aspect ratios: discrepancies between experimental and theoretical results. *ASME Paper* 85-HT-37.

LEE, Y. 1981 Numerical study of multicellular natural convection in vertical cavities. Ph.D. dissertation, The Ohio State University.

LEE, Y. & KORPELA, S. A. 1983 Multicellular convection in a vertical slot. *J. Fluid Mech.* **126**, 91–121.

LEE, Y., KORPELA, S. A. & HORNE, R. N. 1982 Structure of multicellular natural convection in a tall vertical annulus. In *Heat Transfer 1982, Proc. 7th Intl Heat Trans. Conf., Munich*, vol. 2, pp. 221–226. Hemisphere.

LINTHORST, S. J. M., SCHINKEL, W. M. M. & HOOGENDORN, C. J. 1981 Flow structure with natural convection in inclined air-filled enclosures. *Trans. ASME* C: *J. Heat Transfer* **103**, 535–539.

OSTRACH, S., LOKA, R. R. & KUMAR, A. 1980 Natural convection in low aspect-ratio rectangular enclosures. In *19th Natl Heat Transfer Conf., Orlando, ASME HTD*, vol. 8, pp. 1–10.

QUON, C. 1972 High Rayleigh number convection in an enclosure – a numerical study. *Phys. Fluids* **15**, 12–19.

ROACHE, P. J. 1972 *Computational Fluid Dynamics*. Hermosa.

ROUX, B., BONTOUX, P. & HENRY, D. 1984 Numerical and theoretical study of different flow regimes occurring in horizontal fluid layers, differentially heated. In *Macroscopic Modelling of Turbulent Flows* (ed. U. Frisch, J. B. Keller, G. C. Papanicolaou & O. Pironneau). Lecture Notes in Physics, vol. 230, pp. 202–217. Springer.

RUDAKOV, R. N. 1967 Spectrum of perturbations and stability of convective motion between vertical planes. *Prikl. Math. Mekh.* **31**, 349–355.

RUTH, D. 1979 On the transition to transverse rolls in an infinite vertical fluid layer – a power series solution. *Intl J. Heat Mass Transfer* **22**, 1199–1209.

SAID, M. N. A. & TRUPP, A. C. 1979 Laminar free convection in small aspect ratio enclosures with isothermal boundary conditions. *Trans. ASME* C: *J. Heat Transfer* **101**, 569–571.

SCHINKEL, W. M. M. 1980 Natural convection in inclined air-filled enclosures. Ph.D. dissertation, Delft University.

SEKI, N., FUKUSAKO, S. & INABA, H. 1978 Visual observation of natural convective flow in a narrow vertical cavity. *J. Fluid Mech.* **84**, 695–704.

SERNAS, V. & LEE, E. I. 1981 Heat transfer in air enclosures of aspect ratio less than one. *Trans. ASME* C: *J. Heat Transfer* **103**, 617–622.

SHIRALKAR, G. S., GADGIL, A. & TIEN, C. L. 1981 High Rayleigh number convection in shallow enclosures with different end temperatures. *Intl J. Heat Mass Transfer* **24**, 1621–1629.

SHIRALKAR, G. S. & TIEN, C. L. 1981 A numerical study of laminar natural convection in shallow cavities. *Trans. ASME* C: *J. Heat Transfer* **103**, 226–231.

SIMPKINS, P. G. & DUDDERAR, J. D. 1981 Convection in rectangular cavities with differentially heated end walls. *J. Fluid Mech.* **110**, 433–456.

VEST, C. M. & ARPACI, V. S. 1969 Stability of natural convection in a vertical slot. *J. Fluid Mech.* **36**, 1–15.

WIRTZ, R. A. & LIU, L. H. 1975 Numerical experiments on the onset of layered convection in a narrow slot containing a stably stratified fluid. *Intl J. Heat Mass Transfer* **18**, 1299–1305.

WIRTZ, R. A., RIGHI, J. & ZIRILLI, F. 1982 Measurement of natural convection across tilted rectangular enclosures of aspect ratio 0.1 and 0.2. *Trans. ASME* C: *J. Heat Transfer* **104**, 521–526.

WIRTZ, R. A. & TSENG, W. 1979 A finite difference simulation of free convection in tilted enclosures of low aspect ratio. In *Numerical Methods in Thermal Problems*, vol. I, pp. 381–390. Pineridge.

WIRTZ, R. A. & TSENG, W. 1980 Natural convection across tilted rectangular enclosures of small aspect ratio. In *19th Nat Heat Transfer Conf., ASME HTD*, vol. 8, pp. 47–54.